

# High-fidelity readout and control of a nuclear spin qubit in silicon

Jarryd J. Pla<sup>1</sup>, Kuan Y. Tan<sup>1†</sup>, Juan P. Dehollain<sup>1</sup>, Wee H. Lim<sup>1†</sup>, John J. L. Morton<sup>2</sup>, Floris A. Zwanenburg<sup>1‡</sup>, David N. Jamieson<sup>3</sup>, Andrew S. Dzurak<sup>1</sup> & Andrea Morello<sup>1</sup>

**Detection of nuclear spin precession is critical for a wide range of scientific techniques that have applications in diverse fields including analytical chemistry, materials science, medicine and biology. Fundamentally, it is possible because of the extreme isolation of nuclear spins from their environment. This isolation also makes single nuclear spins desirable for quantum-information processing, as shown by pioneering studies on nitrogen-vacancy centres in diamond<sup>1–4</sup>. The nuclear spin of a <sup>31</sup>P donor in silicon is very promising as a quantum bit<sup>5</sup>: bulk measurements indicate that it has excellent coherence times<sup>6,7</sup> and silicon is the dominant material in the microelectronics industry. Here we demonstrate electrical detection and coherent manipulation of a single <sup>31</sup>P nuclear spin qubit with sufficiently high fidelities for fault-tolerant quantum computing<sup>8</sup>. By integrating single-shot readout of the electron spin<sup>9</sup> with on-chip electron spin resonance<sup>10</sup>, we demonstrate quantum non-demolition<sup>11</sup> and electrical single-shot readout of the nuclear spin with a readout fidelity higher than 99.8 per cent—the highest so far reported for any solid-state qubit. The single nuclear spin is then operated as a qubit by applying coherent radio-frequency pulses. For an ionized <sup>31</sup>P donor, we find a nuclear spin coherence time of 60 milliseconds and a one-qubit gate control fidelity exceeding 98 per cent. These results demonstrate that the dominant technology of modern electronics can be adapted to host a complete electrical measurement and control platform for nuclear-spin-based quantum-information processing.**

Quantum computers have the potential to revolutionize aspects of modern society, ranging from fundamental science to information technology<sup>12</sup>. The successful demonstration of such a machine requires the ability to perform high-fidelity control and measurement of individual qubits—the building blocks of a quantum computer. Errors introduced by quantum operations and measurements can be mitigated by using quantum error correction protocols, provided that the probabilities of the errors occurring are below certain stringent thresholds<sup>8</sup>. State-of-the-art high-fidelity qubit control and readout has been realized using laser-cooled atoms in electromagnetic traps<sup>13,14</sup>—a result made possible because of their extreme isolation in a near-perfect vacuum.

Qubits based on solid-state physical systems<sup>15,16</sup> are attractive because of the potential for scalability using modern integrated-circuit fabrication technologies. However, they tend to exhibit much lower system fidelities owing to interactions with their host environment. The ability to combine the control and measurement fidelities of trapped atoms with the scalability inherent to solid-state implementations is therefore highly desirable. The nuclear spin of a single atom is promising in this regard as it is a simple, well-isolated quantum system. One of the earliest proposals for quantum computing in the solid state advocated using the nuclear spin of individual <sup>31</sup>P dopant atoms in silicon to encode and process quantum information<sup>5</sup>. Silicon is an

excellent platform for spin-based quantum-information processing because it can be enriched in the nuclear-spin-zero <sup>28</sup>Si isotope<sup>17</sup>, providing an effective ‘semiconductor vacuum’ and very long spin coherence times. Experiments in bulk phosphorus-doped isotopically enriched silicon (<sup>28</sup>Si:P) have demonstrated the potential of this system in which the <sup>31</sup>P nuclear spin has been used as a quantum memory<sup>7</sup> and as a qubit with extraordinarily long coherence lifetimes of over 180 s (ref. 6). However, owing to detection limitations, experiments have so far been carried out on only large ensembles of <sup>31</sup>P nuclei typically consisting of several billion nuclear spins<sup>6,18</sup>. To realize nuclear-spin-based solid-state quantum computing, one must first isolate, measure and control individual nuclear spins.

It is challenging to measure the state of a single nuclear spin owing to its weak magnetic moment. In the solid state, this has been achieved only for the nitrogen-vacancy centre in diamond<sup>2</sup>, with optical detection, and for a rare-earth terbium ion by performing electrical transport measurements through a single molecule<sup>19</sup>. In both these cases, a coupled electron spin was used to read out the nuclear spin, which requires the ability to measure a single electron spin. The same applies to the <sup>31</sup>P nucleus: the high-fidelity single-shot readout of the donor-bound electron spin<sup>9</sup> is at the heart of our nuclear spin readout method.

We use an on-chip all-electrical detection method for both electron and nuclear spins, using a compact nanoscale device<sup>20</sup> (Fig. 1a) compatible with silicon metal–oxide–semiconductor fabrication standards. The device consists of ion-implanted phosphorus donors<sup>21</sup>, tunnel coupled to a silicon metal–oxide–semiconductor single-electron transistor (SET)<sup>22</sup>.

The <sup>31</sup>P donor in silicon possesses a nuclear spin  $I$  of 1/2, and at cryogenic temperatures it can bind an electron (with spin  $S = 1/2$ ) in the neutral  $D^0$  donor charge state. Therefore, a single <sup>31</sup>P donor constitutes a two-qubit system, where the two qubits interact with an external magnetic field  $B_0$  in proportion to their gyromagnetic ratios:  $\gamma_n = 17.23 \text{ MHz T}^{-1}$  for the nucleus<sup>23</sup> and  $\gamma_e = g\mu_B/h = 27.97 \text{ GHz T}^{-1}$  for the electron, where  $g = 1.9985$  (ref. 24) is the Landé  $g$ -factor,  $\mu_B$  is the Bohr magneton and  $h$  is Planck’s constant. In addition, they interact with each other through the hyperfine interaction  $A = 117.53 \text{ MHz}$  (ref. 24) that arises from the overlap between the wavefunctions of the electron and the <sup>31</sup>P nucleus. If  $\gamma_e B_0 \gg A > 2\gamma_n B_0$ , the eigenstates of the two-spin system are approximately (in ascending order of energy)  $|\downarrow\uparrow\rangle, |\downarrow\downarrow\rangle, |\uparrow\downarrow\rangle$  and  $|\uparrow\uparrow\rangle$ , where the thin (thick) arrow indicates the orientation of the electron (nuclear) spin (Fig. 1b). The system can be transformed to that of a single <sup>31</sup>P nuclear spin (Fig. 1c) with eigenstates  $|\uparrow\rangle$  and  $|\downarrow\rangle$  by using the nanostructure device (Fig. 1a) to ionize the donor to the  $D^+$  charge state.

The <sup>31</sup>P nuclear spin readout experiment begins by performing electron spin resonance (ESR) on its bound donor electron<sup>10</sup>, using microwave pulses delivered by an on-chip broadband planar transmission line<sup>25</sup>. The system exhibits two possible ESR frequencies,

<sup>1</sup>Centre for Quantum Computation and Communication Technology, School of Electrical Engineering and Telecommunications, University of New South Wales, Sydney, New South Wales 2052, Australia.

<sup>2</sup>London Centre for Nanotechnology, University College London, London WC1H 0AH, UK. <sup>3</sup>Centre for Quantum Computation and Communication Technology, School of Physics, University of Melbourne, Melbourne, Victoria 3010, Australia. †Present addresses: QCD Labs, COMP Centre of Excellence, Department of Applied Physics, Aalto University, PO Box 13500, FI-00076 Aalto, Finland (K.Y.T.); Asia Pacific University of Technology and Innovation, Technology Park Malaysia, Bukit Jalil, 57000 Kuala Lumpur, Malaysia (W.H.L.); NanoElectronics Group, MESA+ Institute for Nanotechnology, University of Twente, 7500 AE Enschede, The Netherlands (F.A.Z.).

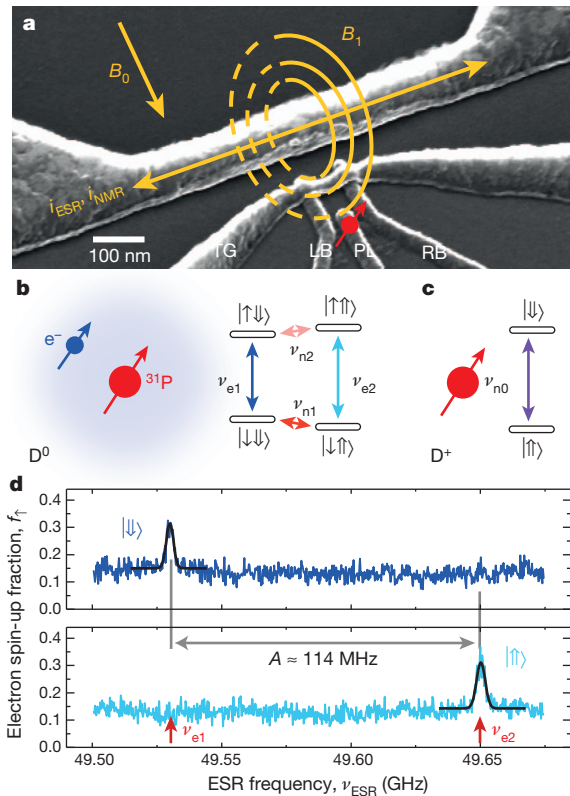


**Figure 1 | Qubit nanostructure, spin transitions and electron spin resonance spectra.** **a**, Scanning electron micrograph of the active area of the qubit device, showing an implanted donor (donor as red arrow), the single-electron transistor (SET) and the short-circuit termination of the microwave line. The device is mounted in a dilution refrigerator with an electron temperature of  $\sim 300$  mK, and is subjected to static magnetic fields  $B_0$  between 1.0 T and 1.8 T.  $B_0$  is oriented perpendicular to the short-circuit termination of the microwave line (solid orange single-ended arrow), which carries a current (solid double-ended arrow) and produces an oscillating magnetic field  $B_1$  (represented by the solid and dashed circles) perpendicular to the surface of the device. TG, top gate; PL, plunger gate; LB, left barrier; RB, right barrier. **b**, Energy-level diagram of the neutral  $^{31}\text{P}$  donor system, with corresponding transitions for electron spin resonance (ESR) in blue, and for nuclear magnetic resonance (NMR) in red.  $\uparrow\downarrow$ : electron spin states;  $\downarrow\downarrow$ : nuclear spin states. **c**, Energy-level diagram of the ionized  $^{31}\text{P}$  donor, with the single NMR transition shown in purple. **d**, ESR spectra obtained at  $B_0 = 1.77$  T by scanning the microwave frequency and monitoring the electron-spin-up fraction  $f_{\uparrow}$ . The top trace corresponds to an active  $\nu_{e1}$  ESR transition (nuclear spin state  $|\downarrow\downarrow\rangle$ ) and the bottom trace to an active  $\nu_{e2}$  ESR transition (nuclear spin state  $|\uparrow\uparrow\rangle$ ).

depending on the state of the nuclear spin:  $\nu_{e1} \approx \gamma_e B_0 - A/2$  for nuclear spin  $|\downarrow\downarrow\rangle$  and  $\nu_{e2} \approx \gamma_e B_0 + A/2$  for nuclear spin  $|\uparrow\uparrow\rangle$ . In a single-atom experiment, if we assume that the ESR measurement duration is much shorter than the nuclear spin flip time, then we expect only one active ESR frequency at any instant. Detecting ESR at the frequency  $\nu_{e1}$  therefore indicates that the nuclear spin is in state  $|\downarrow\downarrow\rangle$ , whereas detection at  $\nu_{e2}$  implies the nuclear spin is  $|\uparrow\uparrow\rangle$ .

Having identified the two resonance frequencies through an ESR experiment (see Fig. 1d and also ref. 10), we performed repeated measurements of the nuclear spin state (Fig. 2a) by toggling the microwave frequency  $\nu_{\text{ESR}}$  between  $\nu_{e1}$  and  $\nu_{e2}$ , obtaining the electron-spin-up fraction  $f_{\uparrow}$  at each point (see Supplementary Information). If the quantity  $\Delta f_{\uparrow} = f_{\uparrow}(\nu_{e2}) - f_{\uparrow}(\nu_{e1})$  is positive, we assign the nuclear state  $|\uparrow\uparrow\rangle$ , and vice versa. A histogram of  $\Delta f_{\uparrow}$  (Fig. 2d) shows two well-separated Gaussian peaks, corresponding to the two possible nuclear orientations, with widths determined by the signal-to-noise ratio (SNR) of the measurements (Supplementary Information). The nuclear spin readout error (Fig. 2e) is obtained by fitting the two peaks and integrating

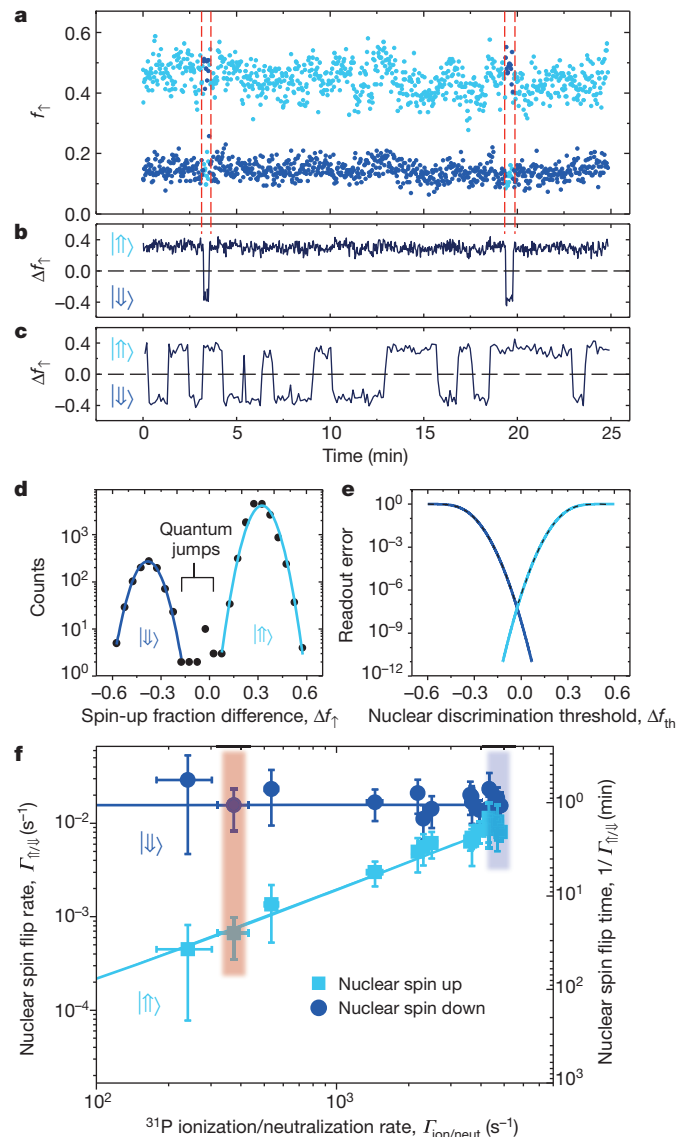


**Figure 2 | Nuclear spin quantum jumps, readout error and lifetimes.**

**a**, Repetitive single-shot measurements of the nuclear spin state performed by toggling  $\nu_{\text{ESR}}$  between  $\nu_{e1} = 49.5305$  GHz (dark blue) and  $\nu_{e2} = 49.6445$  GHz (light blue) and recording the electron-spin-up fraction  $f_{\uparrow}$ . Each data point represents the average  $f_{\uparrow}$  over 250 single-shot measurements of the electron spin (acquired in 260 ms). The electron-tunnelling time is of the order of 100  $\mu\text{s}$ , as reported in ref. 10. The dashed red lines indicate instants when a nuclear spin quantum jump has occurred. **b**, Electron-spin-up fraction difference,  $\Delta f_{\uparrow} = f_{\uparrow}(\nu_{e2}) - f_{\uparrow}(\nu_{e1})$ , for the data in **a**.  $\Delta f_{\uparrow} > 0$  indicates nuclear spin  $|\uparrow\uparrow\rangle$ , and vice versa. **c**,  $\Delta f_{\uparrow}$  in an experiment with an increased rate of donor ionization/neutralization,  $\Gamma_{\text{ion/neutral}}$ . The greater  $\Gamma_{\text{ion/neutral}}$  is achieved by including an additional phase in the nuclear spin readout measurement, where resonant tunnelling of  $|\downarrow\rangle$  electrons between the donor and SET occurs (see Supplementary Information). **d**, Histograms of  $\Delta f_{\uparrow}$  for the data in **b**, showing two well-separated Gaussian peaks, each corresponding to a nuclear spin state, as indicated. The counts obtained for  $-0.015 < \Delta f_{\uparrow} < 0.05$  are attributed to nuclear spin quantum jumps occurring during the measurement. The light and dark blue solid lines are Gaussian fits to the data (see discussion in main text). **e**, Readout errors as a function of the detection threshold for  $\Delta f_{\uparrow}$ . The solid dark (light) blue line indicates the SNR-limited error for detecting the  $|\downarrow\downarrow\rangle$  ( $|\uparrow\uparrow\rangle$ ) state, whereas the black dashed line indicates the total error. **f**, Nuclear spin flip rates  $\Gamma_{\uparrow/\downarrow}$  as a function of the donor ionization/neutralization rate  $\Gamma_{\text{ion/neutral}}$ . The light blue line is a fit to  $\Gamma_{\uparrow} = \Gamma_0 + p\Gamma_{\text{ion/neutral}}$ , with  $p = 1.91(8) \times 10^{-6}$ . The dark blue line is a constant  $\Gamma_{\downarrow} = 1.54(17) \times 10^{-2} \text{ s}^{-1}$ . The red and blue shaded regions indicate the values obtained from the data sets in **b** and **c**, respectively. The error bars represent a 95% confidence level (see Supplementary Information).

each Gaussian beyond a discrimination threshold  $\Delta f_{\text{th}}$ . At the optimal value of  $\Delta f_{\text{th}} = -0.025$ , the SNR-limited readout error is  $2 \times 10^{-7}$ .

We observe that the nuclear spin state remains unchanged for several minutes before exhibiting a ‘quantum jump’ to the opposite state<sup>2</sup>. It is also evident (Fig. 2b) that the nuclear spin is predominantly oriented in the  $|\uparrow\rangle$  state, which we attribute to an electron–nuclear spin flip-flop process, in which the energy difference  $E_{\uparrow\downarrow} - E_{\downarrow\uparrow}$  (that is, between states  $|\uparrow\downarrow\rangle$  and  $|\downarrow\uparrow\rangle$ ) is released to the phonon bath<sup>18,26</sup>. Because  $E_{\uparrow\downarrow} - E_{\downarrow\uparrow} \gg k_B T$  in our experiment, this process acts only in the direction  $|\uparrow\downarrow\rangle \rightarrow |\downarrow\uparrow\rangle$  (that is, only spontaneous emission of phonons occurs), and it cannot be responsible for the observed nuclear spin jumps from  $|\uparrow\rangle$  to  $|\downarrow\rangle$ . We have verified that the  $|\uparrow\rangle \rightarrow |\downarrow\rangle$  transition originates from the readout process, where the donor undergoes repeated ionization and neutralization events. These events result in a

time-varying Hamiltonian, where the exact nature of the nuclear eigenstates varies slightly between the neutral and the ionized donor case. Accordingly, we observe (Fig. 2c, f) that the lifetime of the nuclear spin  $|\uparrow\rangle$  is inversely proportional to the rate of ionization and neutralization (see also Supplementary Information).

By exploiting the broadband nature of our on-chip microwave transmission line, we perform a nuclear magnetic resonance (NMR) experiment (see Supplementary Information for details) on the  $^{31}\text{P}$  nuclear spin (Fig. 3a). For a neutral donor, we expect two NMR frequencies depending on the state of the electron:  $\nu_{n1} = A/2 + \gamma_n B_0$  when the electron spin is  $|\downarrow\rangle$  and  $\nu_{n2} = A/2 - \gamma_n B_0$  when the electron spin is  $|\uparrow\rangle$  (Fig. 1b). However, we can also perform an NMR experiment while the donor is ionized (Fig. 1c), as recently demonstrated in a bulk Si:P sample<sup>27</sup>. In this case there is only one resonance frequency:

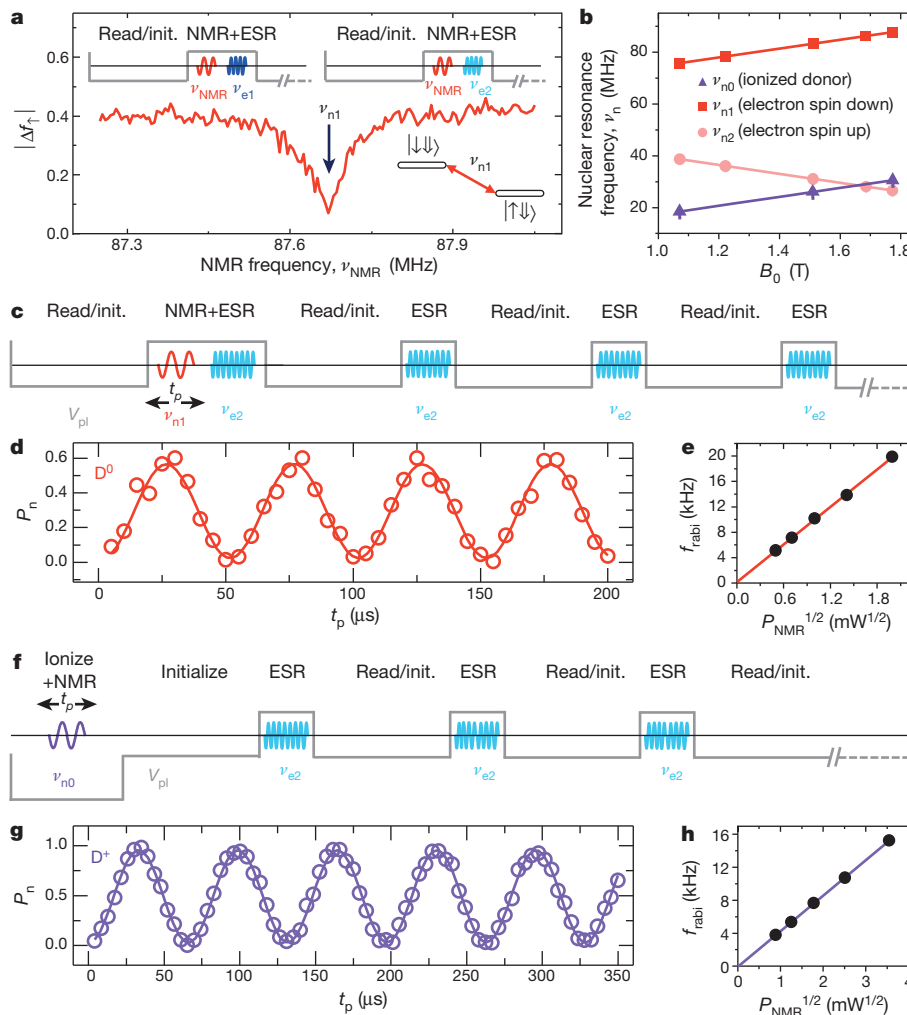


**Figure 3 | NMR spectra and Rabi oscillations of a single  $^{31}\text{P}$  nuclear spin.**

**a**, Observation of nuclear resonance at  $B_0 = 1.77$  T, while the electron spin is initialized  $|\downarrow\rangle$  (see Supplementary Information). The top inset shows the plunger gate voltage waveform (grey line) plus NMR/ESR pulse sequence, and the bottom-right inset shows the energy levels involved in the NMR transition. **b**, Dependence of the NMR resonances  $\nu_{n0}$ ,  $\nu_{n1}$  and  $\nu_{n2}$  on the magnetic field  $B_0$ . Solid lines are the values predicted using the  $^{31}\text{P}$  nuclear gyromagnetic ratio  $\gamma_n = 17.23$  MHz  $\text{T}^{-1}$ . **c**, Pulse sequence for the coherent rotation of a  $^{31}\text{P}$  nuclear spin with the donor in the neutral  $\text{D}^0$  state. Depicted is the plunger gate voltage waveform (grey line) and combined NMR/ESR pulses. After a coherent NMR pulse at  $\nu_{n1}$  of duration  $t_p$ , the nuclear spin state is read by probing the  $\nu_{e2}$  ESR transition with 300 single-shot adiabatic inversion and electron-spin readout measurements, lasting approximately 300 ms. The resulting electron-spin-up fraction  $f_e(\nu_{e2})$  is compared to a threshold, extracted from the quantum jump experiment (Fig. 2a), and a nuclear spin orientation is ascribed to the measurement. **d**, Rabi oscillation

of the neutral  $^{31}\text{P}$  donor nuclear spin with  $P_{\text{NMR}} = 4$  mW,  $B_0 = 1.07$  T and  $\nu_{n1} = 75.7261$  MHz. The pulse sequence of **c** is repeated 40 times for each Rabi pulse length  $t_p$ , with five sweeps of  $t_p$  performed to give a total of 200 measurements at each  $t_p$ . The number of nuclear spin flips is recorded to give the flip probability  $P_n$ . The solid line is a fit of the form  $P_n = K \sin^2(\pi f_{\text{Rabi}} t_p)$ , where  $K$  and  $f_{\text{Rabi}}$  are free fitting parameters. **e**, Rabi frequency, extracted from fits of data similar to that in **d**, against the square root of the radio-frequency power.

**f**, Modified pulse sequence to perform Rabi oscillations on the  $^{31}\text{P}$  nuclear spin with the donor in the ionized  $\text{D}^+$  state. The electron is removed before applying a coherent NMR burst. The electron is then replaced so that a single-shot measurement can be performed on the nuclear spin. **g**, Sample Rabi oscillation of the ionized donor nuclear spin using  $P_{\text{NMR}} = 126$  mW,  $B_0 = 1.77$  T and  $\nu_{n0} = 30.5485$  MHz, with each data point again obtained from 200 measurements of the nuclear spin state. **h**, Plot showing the linear variation of the ionized nuclear spin Rabi frequency with the excitation amplitude.

$\nu_{n0} = \gamma_n B_0$ . Figure 3b shows the magnetic-field dependence of the three NMR frequencies, which agree with the expected values assuming the bulk  $^{31}\text{P}$  gyromagnetic ratio  $\gamma_n = 17.23 \text{ MHz T}^{-1}$  (ref. 23). Furthermore, we extract  $g = 1.9987(6)$  (see Supplementary Information), which is within about 0.01% of the bulk value for Si:P, whereas the hyperfine splitting  $A = 114.30(1) \text{ MHz}$  is Stark shifted<sup>5</sup> from the bulk value of 117.53 MHz (ref. 24). The observation of a Stark shift of  $A$  is important, as it has been proposed<sup>5</sup> as a mechanism to address individual  $^{31}\text{P}$  nuclear spin qubits while applying a global microwave field.

Having found the NMR frequencies, we use short radio-frequency pulses to produce coherent superpositions of the nuclear spin states. For the neutral ( $\text{D}^0$ ) donor, we first initialize the electron in the  $|\downarrow\rangle$  state. A pulse of length  $t_p$  and at the  $\nu_{n1}$  resonance is applied immediately after, followed by a single-shot readout of the nuclear spin state (see Fig. 3c). Measuring the nuclear spin flip probability  $P_n$  as a function of  $t_p$  results in the coherent Rabi oscillations of Fig. 3d, whose frequency  $f_{\text{rabi}}$  scales linearly with the square root of the radio-frequency excitation power,  $P_{\text{NMR}}^{1/2}$  (Fig. 3e). The visibility of the oscillations in Fig. 3d is  $\sim 60\%$ . Deviations from ideality are most probably due to erroneous electron initialization in the excited  $|\uparrow\rangle$  state<sup>10</sup>, caused by heating resulting from the train of microwave pulses used during readout. We modified the pulse sequence to remove the electron before applying the radio-frequency excitation at the  $\nu_{n0}$  transition (Fig. 3f). The Rabi oscillations on the ionized ( $\text{D}^+$ )  $^{31}\text{P}$  nuclear spin (Fig. 3g, h) have near-unity visibility, as the electron spin state has no bearing on the nuclear resonance frequency while the donor is ionized.

To assess the viability of using the  $^{31}\text{P}$  nuclear spin as a quantum bit, it is critical to characterize the duration over which coherence is preserved. The dephasing time  $T_2^*$  is obtained from a Ramsey-fringe measurement (see Supplementary Information), the NMR pulse sequence for which is shown in Fig. 4a (see also Fig. 4b for a Bloch sphere state evolution). The decay of the oscillations in Fig. 4c, with increasing inter-pulse delay  $\tau$ , is the result of fluctuations in the local magnetic environment. Fitting the data with a damped cosine function  $P_n(\tau) = P_n(0)\cos(2\pi\Delta\tau)\exp(-\tau/T_2^*)$ , where  $P_n(0)$  is the amplitude and  $\Delta\tau$  is the average detuning from resonance, reveals  $T_2^*(\text{D}^0) = 0.84(10) \text{ ms}$  for the neutral donor and  $T_2^*(\text{D}^+) = 3.3(3) \text{ ms}$  for the ionized donor. These dephasing times are  $\sim 10^4$  times longer than those measured for the electron spin<sup>10</sup>.

As many of the magnetic fluctuations that contribute to  $T_2^*$  occur on much longer timescales than the typical nuclear spin manipulation time ( $\sim 25 \mu\text{s}$  for a  $\pi$  pulse), a significant portion of the dephasing can be reversed by using spin-echo techniques (Fig. 4d, e). Observing the echo signal while varying the delay  $\tau$  yields the decay curves displayed in Fig. 4f. We fit the data with functions of the form  $y = y(0)\exp[-(2\tau/T_2)^b]$ , where  $y(0)$  is the amplitude,  $b$  is a free exponent and  $T_2$  is the coherence time. For the ionized donor spin, we extract  $T_2(\text{D}^+) = 60.0(9) \text{ ms}$  and  $b(\text{D}^+) = 1.77(7)$ , both of which are fully accounted for by the spectral diffusion caused by dynamics of the  $^{29}\text{Si}$  nuclear spin bath, as quantified by recent theory<sup>28</sup>. Accordingly, we expect that removal of  $^{29}\text{Si}$  through isotopic purification<sup>17</sup> should yield  $T_2$  values of the order of minutes, as observed in bulk-doped samples<sup>6</sup>.

Conversely, for the neutral donor spin, we find a shorter  $T_2(\text{D}^0) = 3.5(1) \text{ ms}$  and  $b(\text{D}^0) = 2.2(2)$ . This suggests that additional decoherence processes occur in the presence of the donor-bound electron. Charge noise at the Si/SiO<sub>2</sub> interface<sup>27</sup> or electronic gate noise<sup>5</sup> could cause a time-dependent Stark shift of the hyperfine coupling, resulting in fluctuations of the instantaneous nuclear Larmor frequency. Ionizing the donor thus removes the connection between the electrical noise and the nuclear spin precession frequency. This is a static effect, in contrast to a recent experiment on the nitrogen-vacancy centre in diamond<sup>3</sup>, where rapid ionization and neutralization improved the coherence of a  $^{13}\text{C}$  nuclear spin through motional averaging.

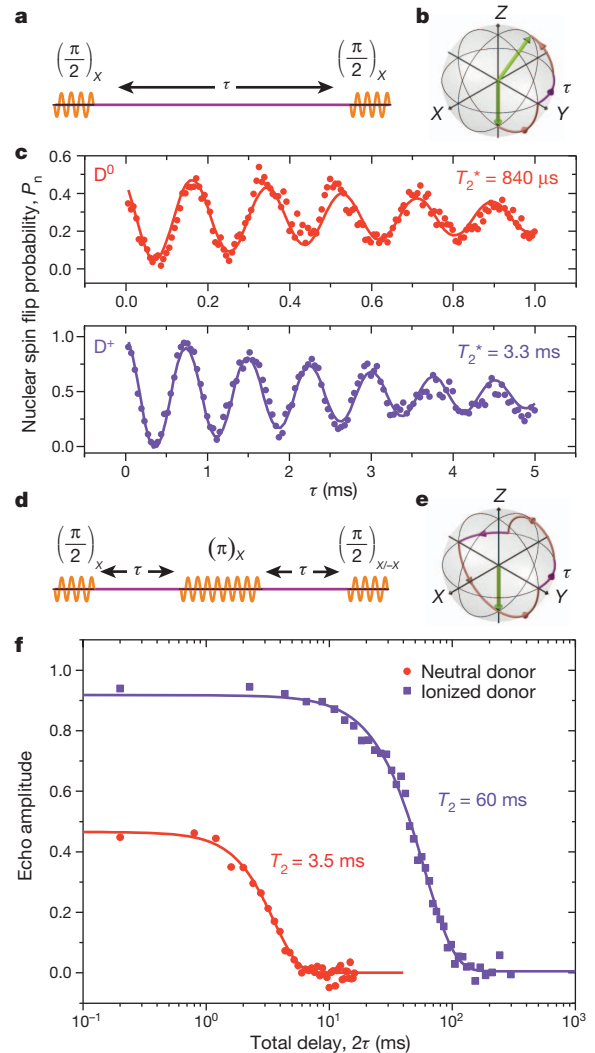


**Figure 4 | Ramsey fringes and spin-echo decay.** **a**, NMR pulse sequence for the Ramsey-fringe experiment. This sequence replaces the single pulse of duration  $t_p$  in Fig. 3c (Fig. 3f) for the neutral (ionized) donor, whereas the nuclear spin is read out in the same way. The phase of both  $\pi/2$  pulses is such that rotation is performed about the  $X$  axis on the Bloch sphere, as noted in the rotation angle subscript above each pulse. **b**, Bloch-sphere representation of the evolution in the rotating frame for the Ramsey-fringe measurement. The green arrow represents the nuclear spin. The purple path indicates dephasing in between pulses, whereas the orange path represents a rotation about the  $X$  axis. **c**, Ramsey interference fringes for the nuclear spin with the donor in the  $\text{D}^0$  (top) and  $\text{D}^+$  (bottom) charge states, taken at  $B_0 = 1.77 \text{ T}$ . Here a  $\pi/2$  pulse was  $12.5 \mu\text{s}$  for the  $\text{D}^0$  experiment and  $23.5 \mu\text{s}$  for the  $\text{D}^+$  experiment. We sweep the inter-pulse delay, and repeat the sequence 20 times at each  $\tau$ . Ten sweeps are performed (with the total 200 measurements occurring over  $\sim 3 \text{ min}$  for each  $\tau$ ) and the nuclear spin flip probability  $P_n$  is found. Fits to the data are discussed in the main text. **d**, NMR pulse sequence for the spin-echo experiment. Here we also implement phase cycling, where the final  $\pi/2$  rotation is first performed about the  $X$  axis and the measurement is then repeated with the final  $\pi/2$  rotation about the  $-X$  axis. Subtracting the two signals ensures a baseline of zero. **e**, Bloch-sphere representation of the spin-echo measurement. Here the final  $\pi/2$  pulse is about the  $X$  axis (the  $-X$  axis is not shown). **f**, Decay of the echo amplitude as the delay  $\tau$  is increased for the case of a neutral (circles) and ionized (squares) donor. We perform 40 repetitions of the sequence for each  $\tau$  and 25 sweeps, totalling 1,000 measurements at each point. The phase-cycled echo amplitude is given by  $P_n(\nu_n, -X) - P_n(\nu_n, X)$ , where  $P_n(\nu_n, -X/X)$  represents the nuclear spin flip probability measured at the NMR resonance  $\nu_n$  with a final  $\pi/2$  pulse about the  $-X$  or  $X$  axis. All other experimental conditions are as in the Ramsey-fringe experiment. Fits through the data are discussed in the text.

We now analyse the fidelity of our solid-state qubit. Single-shot nuclear spin readout can be performed with extremely high fidelity, owing to the quantum non-demolition (QND)<sup>11</sup> nature of the measurement. The physical phenomena responsible for the observed quantum jumps of the nuclear spin originate from the measurement through the electron spin, and can be viewed as a deviation from QND ideality (see Supplementary Information). For the nuclear  $|\uparrow\rangle$  state, this results in a lifetime of  $T_{\uparrow} = 1,500(360)$  s (obtained from extended data of the measurement in Fig. 2a). For the nuclear  $|\downarrow\rangle$  state, the cross-relaxation process, which is caused by phonons modulating the hyperfine coupling, yields  $T_{\downarrow} = 65(15)$  s (Fig. 2a). These lifetimes must be contrasted with the nuclear-spin measurement time  $T_{\text{meas}}$ , which has been optimized here to maximize the nuclear-spin readout fidelity (see Supplementary Information). Combining the optimal measurement time ( $T_{\text{meas}} = 104$  ms) with the observed nuclear-spin lifetimes yields the QND fidelities:  $F_{\text{QND}}(|\uparrow\rangle) = \exp(-T_{\text{meas}}/T_{\uparrow}) = 0.99993(2)$ ; and  $F_{\text{QND}}(|\downarrow\rangle) = \exp(-T_{\text{meas}}/T_{\downarrow}) = 0.9984(4)$ . We have therefore obtained readout fidelities between 99.8% and 99.99%, the highest reported so far for any solid-state qubit, and comparable with the fidelities observed for qubits in vacuum-based ion-trap systems<sup>13</sup>.

The nuclear spin control fidelity  $F_C$  will ultimately be limited by  $T_2$  and the minimum achievable gate-operation time. We quantify  $F_C$  by directly measuring the rotation-angle error for the ionized donor nuclear spin using multiple-pulse dynamical-decoupling sequences (see Supplementary Information). Such a measurement encompasses extrinsic sources of pulse error, for example due to slow power fluctuations of the radio-frequency source. The extracted maximum uncertainty of  $3^\circ$  for an intended  $\pi$  pulse indicates a lower bound on  $F_C$  of 98%.

The results presented here demonstrate that the nuclear spin of a single  $^{31}\text{P}$  donor could constitute a quantum memory in an electron-spin-based quantum computer<sup>10</sup>, or a high-fidelity qubit in a quantum processor where the nuclear spin is the primary computational element<sup>5</sup>. Future experiments will therefore focus on demonstrating electron–nuclear entanglement<sup>29,30</sup> and the coupling of multiple nuclei mediated by hyperfine and exchange interactions<sup>5</sup>. We anticipate that exploiting the  $^{31}\text{P}$  nuclear spin qubit will open new avenues for large-scale quantum-computer architectures, where the quantum coherence of well-isolated atomic systems is combined with the manufacturability of silicon nanoelectronic devices.

## METHODS SUMMARY

**Device fabrication.** For information relating to the device fabrication, see ref. 10, where it is described in some detail.

**Experimental set-up.** For our voltage pulses, we employed a compensation technique—using an arbitrary waveform generator (Tektronix, AWG520) and an inverting voltage preamplifier—to ensure that the pulsing shifted only the donor electrochemical potentials while keeping the SET island potential constant. The voltage  $V_p$  (see Supplementary Fig. 1b) was applied directly to the top gate, whereas it was inverted and amplified by a factor  $K$  before reaching the plunger gate. The gain  $K$  was carefully tuned to ensure that the SET operating point moved along the top of the SET current peaks, as indicated by the blue arrow in Fig. 1d of ref. 9. The SET current was measured by a Femto DLPCA-200 transimpedance amplifier at room temperature, followed by a voltage post-amplifier, a sixth-order low-pass Bessel filter and a fast digitizing oscilloscope.

The ESR excitations were produced by an Agilent E8257D microwave analogue signal generator and the NMR excitations by an Agilent MXG N5182A radio-frequency vector signal generator. The two signals were combined at room temperature using a power divider/combiner, before being guided to the sample by a semi-rigid coaxial cable (2.2 m in length). Gating of the ESR/NMR pulses was provided by the Tektronix AWG520, which was synchronized with the top gate and plunger gate pulses.

Received 9 December 2012; accepted 13 February 2013.

1. Jelezko, F. *et al.* Observation of coherent oscillation of a single nuclear spin and realization of a two-qubit conditional quantum gate. *Phys. Rev. Lett.* **93**, 130501 (2004).

2. Neumann, P. *et al.* Single-shot readout of a single nuclear spin. *Science* **329**, 542–544 (2010).
3. Maurer, P. C. *et al.* Room-temperature quantum bit memory exceeding one second. *Science* **336**, 1283–1286 (2012).
4. Pfaff, W. *et al.* Demonstration of entanglement-by-measurement of solid-state qubits. *Nature Phys.* **9**, 29–33 (2013).
5. Kane, B. E. A silicon-based nuclear spin quantum computer. *Nature* **393**, 133–137 (1998).
6. Steger, M. *et al.* Quantum information storage for over 180 s using donor spins in a  $^{28}\text{Si}$  semiconductor vacuum. *Science* **336**, 1280–1283 (2012).
7. Morton, J. J. L. *et al.* Solid-state quantum memory using the  $^{31}\text{P}$  nuclear spin. *Nature* **455**, 1085–1088 (2008).
8. Knill, E. Quantum computing with realistically noisy devices. *Nature* **434**, 39–44 (2005).
9. Morello, A. *et al.* Single-shot readout of an electron spin in silicon. *Nature* **467**, 687–691 (2010).
10. Pla, J. J. *et al.* A single-atom electron spin qubit in silicon. *Nature* **489**, 541–545 (2012).
11. Braginsky, V. B., Khalili, F. & Ya. Quantum nondemolition measurements: the route from toys to tools. *Rev. Mod. Phys.* **68**, 1–11 (1996).
12. Nielsen, M. A. & Chuang, I. L. *Quantum Computation and Quantum Information* (Cambridge Univ. Press, 2000).
13. Myerson, A. H. *et al.* High-fidelity read-out of trapped-ion qubits. *Phys. Rev. Lett.* **100**, 200502 (2008).
14. Brown, K. R. *et al.* Single-qubit-gate error below  $10^{-4}$  in a trapped ion. *Phys. Rev. A* **84**, 030303(R) (2011).
15. Clarke, J. & Wilhelm, F. K. Superconducting quantum bits. *Nature* **453**, 1031–1042 (2008).
16. Hanson, R. & Awschalom, D. D. Coherent manipulation of single spins in semiconductors. *Nature* **453**, 1043–1049 (2008).
17. Becker, P., Pohl, H. J., Riemann, H. & Abrosimov, N. Enrichment of silicon for a better kilogram. *Phys. Status Solidi A* **207**, 49–66 (2010).
18. McCamey, D. R., Van Tol, J., Morley, G. W. & Boehme, C. Electronic spin storage in an electrically readable nuclear spin memory with a lifetime > 100 seconds. *Science* **330**, 1652–1656 (2010).
19. Vincent, R., Klyatskaya, S., Ruben, M., Wernsdorfer, W. & Balestro, F. Electronic read-out of a single nuclear spin using a molecular spin transistor. *Nature* **488**, 357–360 (2012).
20. Morello, A. *et al.* Architecture for high-sensitivity single-shot readout and control of the electron spin of individual donors in silicon. *Phys. Rev. B* **80**, 081307(R) (2009).
21. Jamieson, D. N. *et al.* Controlled shallow single-ion implantation in silicon using an active substrate for sub-20-keV ions. *Appl. Phys. Lett.* **86**, 202101 (2005).
22. Angus, S. J., Ferguson, A. J., Dzurak, A. S. & Clark, R. G. Gate-defined quantum dots in intrinsic silicon. *Nano Lett.* **7**, 2051–2055 (2007).
23. Steger, M. *et al.* Optically-detected NMR of optically-hyperpolarized  $^{31}\text{P}$  neutral donors in  $^{28}\text{Si}$ . *J. Appl. Phys.* **109**, 102411 (2011).
24. Feher, G. Electron spin resonance experiments on donors in silicon. I. Electronic structure of donors by the electron nuclear double resonance technique. *Phys. Rev.* **114**, 1219–1244 (1959).
25. Dehollain, J. P. *et al.* Nanoscale broadband transmission lines for spin qubit control. *Nanotechnology* **24**, 015202 (2013).
26. Pines, D., Bardeen, J. & Slichter, C. P. Nuclear polarization and impurity-state spin relaxation processes in silicon. *Phys. Rev.* **106**, 489–498 (1957).
27. Dreher, L., Hoehne, F., Stutzmann, M. & Brandt, M. S. Nuclear spins of ionized phosphorus donors in silicon. *Phys. Rev. Lett.* **108**, 027602 (2012).
28. Witzel, W. M., Carroll, M. S., Cywinski, L. & Das Sarma, S. Quantum decoherence of the central spin in a sparse system of dipolar coupled spins. *Phys. Rev. B* **86**, 035452 (2012).
29. Mehring, M., Mende, J. & Scherer, W. Entanglement between an electron and a nuclear spin 1/2. *Phys. Rev. Lett.* **90**, 153001 (2003).
30. Simmons, S. *et al.* Entanglement in a solid-state spin ensemble. *Nature* **470**, 69–72 (2011).

**Supplementary Information** is available in the online version of the paper.

**Acknowledgements** We thank R. P. Starrett, D. Barber, C. Y. Yang and R. Szymanski for technical assistance and A. Laucht, R. Kalra and J. Muhonen for discussions. This research was funded by the Australian Research Council Centre of Excellence for Quantum Computation and Communication Technology (project number CE11E0096) and the US Army Research Office (W911NF-13-1-0024). We acknowledge support from the Australian National Fabrication Facility.

**Author Contributions** K.Y.T. and W.H.L. fabricated the device; D.N.J. designed the P implantation experiments; J.J.P., K.Y.T., J.J.L.M., J.P.D. and F.A.Z. performed the measurements; J.J.P., A.M., A.S.D. and J.J.L.M. designed the experiments and discussed the results; J.J.P. and A.M. analysed the data; and J.J.P. and A.M. wrote the manuscript with input from all co-authors.

**Author Information** Reprints and permissions information is available at [www.nature.com/reprints](http://www.nature.com/reprints). The authors declare no competing financial interests. Readers are welcome to comment on the online version of the paper. Correspondence and requests for materials should be addressed to A.M. ([a.morello@unsw.edu.au](mailto:a.morello@unsw.edu.au)).